JOURNAL OF GEOPHYSICAL RESEARCH, VOL. 88, NO. C6, PAGES 3885–3893, APRIL 20, 1983

Polarized Microwave Radiation Transfer in Precipitating Cloudy Atmospheres: Applications to Window Frequencies

RUNHENG HUANG[1] AND KUO-NAN LIOU

Department of Meteorology, University of Utah, Salt Lake City, Utah 84112

A microwave radiation transfer model taking into account Mie scattering polarization effects is developed for a plane-parallel precipitating cloudy atmosphere. In the model the azimuthally averaged Mie scattering phase matrix elements are expressed in terms of double Legendre polynomial expansion and the cloud temperature is approximated by a linear function of the optical depth. The complete solution of the fundamental transfer equation is derived utilizing the discrete-ordinates method for horizontal and vertical polarization components. Using this model, the brightness temperature and degree of polarization for three microwave window frequencies of 19.35, 37.0, and 85.5 GHz are calculated for a number of rainfall rates over both land and ocean surfaces. We show that the brightness temperature computed for 85.5 GHz using a simple Rayleigh scattering approximation is underestimated by about 7°K for a layer thickness of 4.7 km and a rainfall rate of 5 mm/hr. Effects of the Mie scattering function and nonisothermal cloud structure must both be included for brightness temperature calculations of 37 and 85.5 GHz when thick precipitating clouds are involved. Moreover, we also find that there is a significant degree of polarization for emergent radiation of 19.35 GHz at a zenith angle of 50° under a light rainfall condition over ocean surfaces. Over land surfaces, polarization produced by precipitating clouds is rather small for the three window frequencies. Finally, we show that the existence of ice particles in the upper part of a precipitating cloud largely reduces the upward radiances of the 85.5 GHz frequency.

1. INTRODUCTION

Development of a microwave radiation transfer model for precipitating cloudy atmospheres is of fundamental importance for retrieval and inference of the cloud liquid water content and rainfall rate. While a number of investigations have been carried out to study the transfer of microwave radiation in precipitating cloudy atmospheres utilizing a Rayleigh scattering approximation (see, e.g., *Weinman and Guetter* [1978] and *Liou et al.* [1980]) a complete and general solution for thermal radiation in scattering atmospheres including the polarization effects of Mie particles has not been derived and developed for numerical computations.

In this paper, we wish to develop a microwave radiation transfer model taking into consideration the Mie scattering polarization effect for nonisothermal precipitating clouds in an inhomogeneous atmosphere. The prime objective of this study is to provide a reliable transfer model for the interpretation of the vertical and horizontal brightness temperatures observed in precipitating cloudy atmospheres over both ocean and land with applications to window frequencies.

In section 2 we begin with the fundamental transfer equation including polarization and derive complete solutions for the emergent brightness temperature for nonisothermal clouds by means of the discrete-ordinates method. In section 3 discussions are presented for the selection of optical and atmospheric parameters, and for the double Legendre polynomial expansion and stability of eigenvalues in the context of the discrete-ordinates method. In this section, we also present the importance of the Mie scattering phase function and nonisothermal cloud emission on the emergent brightness temperature by using a number of microwave frequencies. Numerical results for the transfer of 19.35, 37.0, and 85.5 GHz in precipitating cloudy atmospheres as functions of the rainfall rate in terms of two components of the brightness temperature and degree of linear polarization are presented in section 4. Finally, concluding remarks are given in section 5.

2. FORMULATION OF THE TRANSFER OF MICROWAVE RADIATION INCLUDING POLARIZATION

We shall begin with the basic equation governing the transfer of polarized radiation in a plane-parallel horizontally homogeneous scattering layer with internal emission in terms of the Stokes intensity vector in the form

$$\mu \frac{d\mathbf{I}(\tau;\mu,\phi)}{d\tau} = \mathbf{I}(\tau;\mu,\phi) - \frac{\tilde{\omega}_\nu}{4\pi}\int_0^{2\pi}\int_0^1 \mathbf{P}(\mu,\phi;\mu',\phi') \cdot \mathbf{I}(\tau;\mu',\phi')\,d\mu'\,d\phi' - (1-\tilde{\omega}_\nu)\mathbf{B}_\nu \quad (1)$$

where $\mathbf{I} = [I_l, I_r, U, V]$, l and r represent horizontal and vertical polarized components, respectively, $\mathbf{P}$ denotes the four-by-four phase matrix, $\tilde{\omega}_\nu$ is the single scattering albedo, τ is the vertical optical depth, and $\mathbf{B}_\nu$ is the unpolarized thermal emission Stokes vector and is given by $[B_\nu/2, B_\nu/2, 0, 0]$, where $B_\nu(T)$ is the Planck function in the frequency domain for a temperature T.

The scattering phase matrix on the scattering plane is given by

$$\mathbf{P}(\mu,\phi;\mu',\phi') = \mathbf{L}(\pi - i_2)\,\mathbf{M}(\theta)\,\mathbf{L}(-i_1) \quad (2)$$

where Θ is the scattering angle, i_1 and i_2 denote rotational angles (see, e.g., *Liou* [1980]), $\mathbf{L}$ is the transformation

[1] On leave from the Institute of Atmospheric Physics, Academia Sinica, Beijing, China.

Paper number 3C0144.
0148-0227/83/003C-0144$05.00

matrix, and **M** is the scattering matrix derived from the single scattering theory.

We assume that emission from a homogeneous earth surface is either isotropic (unpolarized land) or zenith-angle dependent (polarized ocean), and that clear-air and precipitation are plane-parallel, horizontally homogeneous. With these assumptions in mind, transfer of microwave radiation may be treated as azimuthally independent so that the intensity is only a function of the optical depth and zenith angle. Thus the phase matrix elements needed in the transfer equation are

$$P_{rs}(\mu, \mu') = \frac{1}{2\pi} \int_0^{2\pi} P_{rs}(\mu, \phi; \mu', \phi') d(\phi' - \phi) \qquad (3)$$

$$r, s = 1, 2, 3, 4$$

Dave [1970] showed that the azimuthally averaged phase matrix elements P_{13}, P_{14}, P_{23}, P_{24}, P_{31}, P_{32}, P_{41}, and P_{42} for th Mie scattering case all become zeros. The analysis of the vertically and horizontally polarized intensities are then independent of the U and V components. Thus we write

$$\mu \frac{dI_l(\tau; \mu)}{d\tau} = I_l(\tau, \mu) - \frac{\tilde{\omega}_\nu}{2} \int_{-1}^{1} d\mu' [P_{11}(\mu, \mu') I_l(\tau, \mu') + P_{12}(\mu, \mu') I_r(\tau, \mu')] - (1 - \tilde{\omega}_\nu) B_\nu(T) \qquad (4a)$$

$$\mu \frac{dI_r(\tau; \mu)}{d\tau} = I_r(\tau, \mu) - \frac{\tilde{\omega}_\nu}{2} \int_{-1}^{1} d\mu' [P_{21}(\mu, \mu') I_l(\tau, \mu') + P_{22}(\mu, \mu') I_r(\tau, \mu')] - (1 - \tilde{\omega}_\nu) B_\nu(T) \qquad (4b)$$

The phase matrix elements denoted in (3) subject to (2) depend on the cosine of the incident and emergent angles μ' and μ and may be expanded in double Legendre polynomials as follows:

$$P_{rs}(\mu, \mu') = \sum_{n=0}^{N} \sum_{m=0}^{M} \tilde{\omega}_{nm}{}^{rs} P_m(\mu') P_n(\mu) \qquad r, s = 1, 2 \qquad (5)$$

where the expansion coefficients

$$\tilde{\omega}_{nm}{}^{rs} = \frac{(2n + 1)(2m + 1)}{4} \cdot \int_{-1}^{1} \int_{-1}^{1} P_{rs}(\mu, \mu') P_n(\mu) P_m(\mu') \, d\mu \, d\mu' \qquad (6)$$

We now use the discrete-ordinates method to solve (4*a*) and (4*b*) simultaneously. Upon replacing the integrals by summations according to the Gaussian quadrature and utilizing the double Legendre polynomial expansions for phase matrix elements we obtain two sets of first-order differential equations coupled with $I_l(\tau, \mu_i)$ and $I_r(\tau, \mu_i)$, where $\mu_i = \cos \theta_i$ is the Gaussian quadrature division for the interval $(-1, 1)$ according to the zeros of the even order Legendre polynomial $P_{2N}(\mu)$, and N denotes the number of finite discrete streams employed.

To seek general solutions for I_l and I_r, we first consider the homogeneous parts of these two equations and then derive a particular solution to each of them. Since they are two sets of coupled first order differential equations, the solutions may be written in terms of eigenvalues and eigenvectors. The particular solution is dependent on the internal emission source, $B_\nu(T)$. Following *Weinman and Guetter* [1977] and *Stamnes and Swanson* [1981], we assume that the internal emission of a scattering cloud layer is a linear function of the vertical depth such that

$$B_\nu[T(\tau)] = B_0 + B_1 \tau \qquad (7)$$

where B_0 and B_1 are constants dependent on the temperatures of cloud top and base. Equation (7) represents an approximation to the non-isothermal precipitating cloud. Thus the complete solution of (5) at a series of discrete angles is

$$I_l(\tau, \mu_i) = \sum_{\lambda=1}^{4N} f_\lambda \phi(\mu_i, k_\lambda) e^{-k_\lambda \tau} + a_0(\mu_i) + a_1(\mu_i)\tau \qquad (8a)$$

$$I_r(\tau, \mu_i) = \sum_{\lambda=1}^{4N} g_\lambda \psi(\mu_i, k_\lambda) e^{-k_\lambda \tau} + b_0(\mu_i) + b_1(\mu_i)\tau \qquad (8b)$$

where k_λ represents the eigenvalues for the system of equations, ϕ and ψ are eigenvectors, a_0, a_1, b_0, and b_1 are coefficients corresponding to the particular solution, and f_λ and g_λ are constants of proportionality to be determined from radiation boundary conditions.

Now, we consider an atmosphere containing a cloud layer having a top and base height of z_t ($\tau = 0$) and z_b ($\tau = \tau^*$), respectively. We define the atmospheric transmittance as

$$\mathcal{T}_\nu(\mu_i, z_1, z_2) = \exp\left[-\frac{1}{\mu_i} \int_{z_1}^{z_2} k_\lambda(z) \, dz\right] \qquad (9)$$

where k_λ represents the gaseous volume absorption coefficient (in units of per length). The downward atmospheric intensity incident on the cloud top is simply

$$I_{l,r}(0, -\mu_i) = \frac{1}{\mu_i} \int_{z_t}^{\infty} k_\lambda T(z) \mathcal{T}_\nu(\mu_i, z_t, z) \, dz \qquad (10)$$

Note that since the Planck function B_ν is linearly proportional to the temperature in the microwave region we have replaced it by the atmospheric temperature. The upward atmospheric intensity reaching the cloud bottom is caused by (1) the emission of the underlying surface, (2) the upward radiation contribution from the atmosphere between the cloud and the surface, and (3) the reflection of the downward radiation reaching the surface which includes the cloud contribution. Hence we write

$$I_{l,r}(\tau^*, \mu_i) = \varepsilon_{l,r} T_s \mathcal{T}_\nu(\mu_i, 0, z_b) + \frac{1}{\mu_i} \int_0^{z_b} k_\nu T(z) \mathcal{T}_\nu(\mu_i, z, z_b) \cdot dz + (1 - \varepsilon_{l,r}) \mathcal{T}_\nu(\mu_i, 0, z_b) \left[\frac{1}{\mu_i} \int_0^{z_b} k_\nu T(z) \mathcal{T}_\nu(\mu_i, 0, z) \, dz + I_{l,r}(0, -\mu_i) \mathcal{T}_{l,r}{}^c(-\mu_i) \mathcal{T}_\nu(\mu_i, 0, z_b)\right] \qquad (11)$$

where $\varepsilon_{l,r}$ denotes the surface emissivity, T_s the surface temperature, $\mathcal{T}_{l,r}{}^c$ the downward cloud transmittance and the total optical depth of a scattering cloud layer is given by

$$\tau^* = \int_{z_b}^{z_t} k_\nu \, dz + \beta_e(z_t - z_b)$$

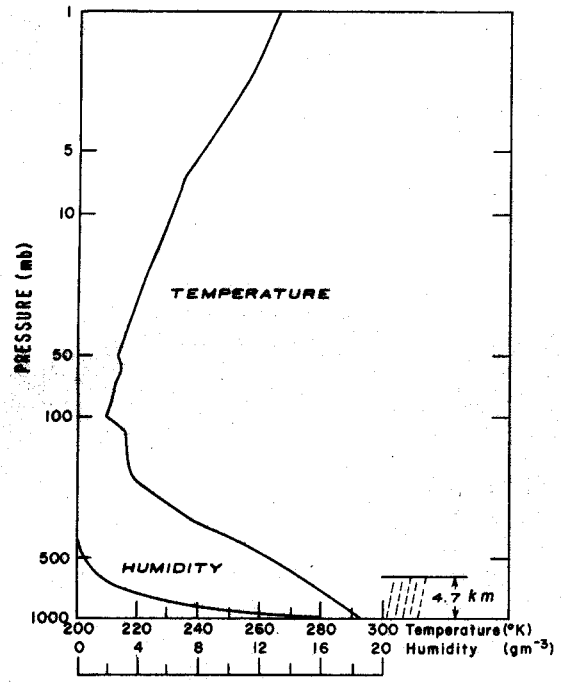

Fig. 1. Climatological temperature and humidity profiles for 30°N, July.

with β_e the extinction coefficient of the cloud particles. Owing to the surface contribution, the boundary intensities at the the bottom of the cloud will be polarized for polarized surfaces.

For remote sensing applications, we shall evaluate the upward intensities at the top of the atmosphere. They are given by

$$I_{l,r}(\infty, \mu_i) = I_{l,r}(z_t, \mu_i)\mathcal{T}_\nu(\mu_i, z_t, \infty) + \frac{1}{\mu_i} \cdot \int_{z_t}^{\infty} k_\nu T(z)\mathcal{T}_\nu(\mu_i, z, \infty)\, dz \qquad (12)$$

where $I_{l,r}(z_t, \mu_i)$ are computed from (8*a*) and (8*b*) when $\tau = 0$ ($z = z_t$). Equation (12) is the basic equation to be used for the investigation of the atmospheric and cloud effects on a number of microwave frequencies. Note that since (8) can also provide the complete solutions in the downward directions, the radiation intensity reaching the ground may be evaluated by using similar procedures.

3. Numerical Computations

3.1. *Selection of Optical and Atmospheric Parameters*

We have developed a microwave radiative transfer program which takes into account the Mie scattering polarization effect of nonisothermal clouds in inhomogeneous atmospheres. The program is general and can be simplified to cases involving the Rayleigh scattering phase function and isothermal clouds over both ocean and land surfaces. The variable parameters involved in the program are the microwave wavelength λ, the rainfall rate R, and the thickness of a precipitating cloud Δz. The surface temperature is taken to be the same as the atmospheric temperature at 1000 mbars. The wavelength covers the microwave window channels, 1.55 cm (19.35 GHz), 0.81 cm (37 GHz), and 0.35 cm (85.5 GHz). The rainfall rate ranges from a light rain (1 mm/hr) to a moderate precipitation (10 mm/hr). The cloud thickness varies from 1.4 km to 4.7 km corresponding to the discrete height of the atmospheric temperature and water vapor profiles used in this study (Figure 1, standard atmosphere for 30°N, July). The *Marshall and Palmer* [1949] raindrop size distribution is used in the single scattering calculations and in the determination of cloud liquid water content.

In order to examine the effect of ice particles in the upper part of clouds on the brightness temperature, we assume a homogeneous ice layer, having the same particle size distribution as the liquid droplets, located above the precipitating cloud. Because there is a substantial difference between scattering properties of liquid droplets and ice spheres, we must solve the transfer equation governing the rain and ice layers separately. We do so by solving the transfer equation of the rain layer first without taking into account the ice layer. Using the upward brightness temperatures at the top of the rain layer as the lower boundary condition, the transfer of microwave radiation through the layer is solved using new scattering parameters for ice spheres. We will show the effects of the ice layer with adjustable thickness on the resultant radiation field in the following section.

An important parameter in the microwave radiation transfer model is the surface emissivity. It is highly variable over land owing to the soil moisture and vegetation, and over sea due to the sea roughness. In general, in the case of land, wetting of the unvegetated soil lowers the surface emissivity. In the case of the sea, the surface wind which increases the roughness increases the emissivity. However, data for the polarization property of the wet soil surface are rather limited. For this reason, an emissivity of 0.96 for dry land and an emissivity of 0.85 for a wet surface [after *Gloersen et al.*, 1972] will be used in this study. For the calm ocean surface we applied the Fresnel reflection formulae to evaluate the vertical and horizontal emissivity components. The real and imaginary refractive indices for pure water involved in the Fresnel formulae were calculated from the equation developed by *Ray* [1972]. For the wind disturbed sea surface, observations [*Webster et al.*, 1976] and theoretical calculations [*Gloersen et al.*, 1972; *Hall*, 1972] showed that over a certain range of surface winds, the emission property of a rough sea is polarized. Observed data presented by Webster et al. are limited to frequencies below 37 GHz and a nadir angle of 38°. Based on the emission intensity of the calm sea surface and the limited emission data we derive an emissivity of the rough sea surface which fits the observations and then extrapolate to other incident angles. While we recognize that the emissivity distribution for rough sea surfaces proposed in this study may not be realistic, such a distribution, however, may provide some qualitative assessment as to how the roughness of the sea surface influences the atmospheric transfer of microwave radiation. The resultant emissivities derived for use in radiative transfer calculations are shown in Figure 2 for a number of microwave frequencies. Results for the rough sea are assumed to be applicable to 37.0 and 85.5 GHz.

To evaluate the clear atmospheric transmittance for microwave radiation we utilized the formulae proposed by *Meeks and Lilley* [1963], *Barrett and Chung* [1962], and *Gaut* [1968] for the absorption and emission of oxygen and water vapor molecules.

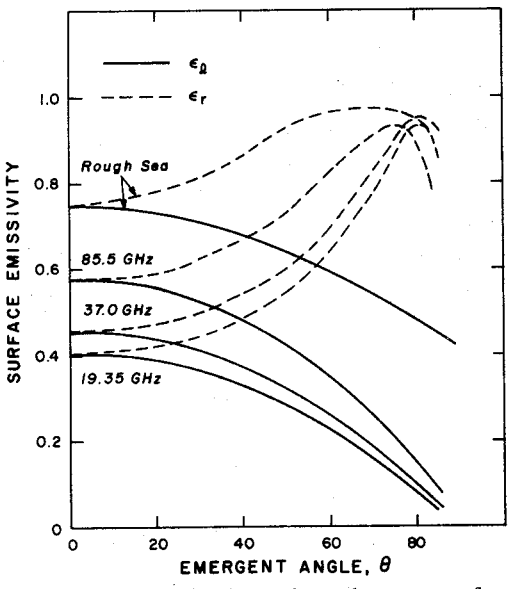

Fig. 2. Emissivities of calm and rough ocean surfaces for a number of microwave frequencies. The solid and dashed curves represent the horizontal ϵ_l and vertical ϵ_r polarization components, respectively.

3.2. *Effects of the Scattering Phase Function on the Brightness Temperature*

One of the objectives of this study is to investigate the precipitation condition under which the Mie scattering theory must be used in the microwave transfer calculation. The effects of scattering processes on the radiative transfer depend on two factors: the relative magnitude of the scattering coefficient to the absorption coefficient (or the single-scattering albedo) and the scattering phase function. The former determines the total scattering intensity, while the latter affects the directional distribution of the scattering field. By using a fixed single-scattering albedo in the transfer calculation, we may examine the brightness temperature differences resulting form the use of Mie and Rayleigh scattering patterns. Figure 3 shows the results for the three frequencies as a function of the rainfall rate using a zenith angle of 0°. A precipitating cloud with a thickness of 4.7 km over ocean was used in the calculation. For 19.35 GHz, differences are insignificant over all the rainfall rates indicated. The negative differences in the case are due to the fact that the Mie scattering phase function has a smaller diffraction peak than the Rayleigh counterpart. The largest difference for 37.0 GHz is less than 2°K when the rainfall rate is within 20 mm/hr. However, for 85.5 GHz the difference increases monotonically with the rainfall rate. It is as much as 7°K for a rainfall rate of 5 mm/hr. The small differences for 19.35 and 37.0 GHz are not because the Mie and Rayleigh scattering functions are similar, but rather because scattering is weak in these cases. It should be noted that for the Marshall-Palmer size distribution the weighted mean droplet radius increases with the rainfall rate through the following relationship

$$\bar{r} = \int_r rn(r)\,dr / \int_r n(r)\,dr \sim R^{0.21}$$

The corresponding mean radius is also given in the abscissa.

3.3. *Effects of the Cloud Temperature Gradient*

The thermal emission source function in the microwave radiative transfer equation is the temperature of the cloud, which, in general, is a function of height or optical depth. In this study we assume that the source function depends linearly on the cloud optical depth. By letting $B_1 = 0$ in (7), the solution reduces to the case of an isothermal cloud. For a nonisothermal cloud, whose temperature is approximately characterized by a linear function in the optical depth, the particular solution of the discrete ordinate equations are the same for two polarization components, i.e., $a_1^i = b_1^i = \text{const}$ and $a_0^i = b_0^i$, where a_0^i is a function of zenith angle.

Figure 4 illustrates the effect of a non-isothermal precipitating cloud with a rainfall rate of 1 mm/hr and a thickness of 4.66 km on two brightness temperature components for a frequency of 37 GHz and 85.5 GHz. It is seen that the emergent brightness temperatures of a nonisothermal cloud are larger than those of an isothermal cloud having the same cloud top temperature. For 37 GHz, the difference is of the order of 3°K. But for 85.5 GHz, it is as much as 5°K. These differences are related to the frequency and cloud thickness used in the calculations. Increasing the cloud thickness increases the brightness temperature differences between these two cases. On the basis of the comparisons in subsections 3.2 and 3.3, the temperature gradient and Mie phase function must be taken into consideration in the microwave transfer calculation for thick precipitating clouds.

4. RESULTS

Figures 5, 6, and 7 illustrate the dependence of the brightness temperature on the rainfall rate for 19.35, 37, and 85.5 GHz channels, respectively. Brightness temperatures for two polarization components at the emergent angle of 50° over both ocean and land surfaces are depicted. A common feature of these figures is that the brightness temperature for these three frequencies increases with the increasing rainfall rate over the ocean surface. The reason is that the ocean is radiometrically cold in the microwave region so that processes of absorption and emission due to precipitating cloud particles dominate. However, it can be seen from these figures that the brightness temperature becomes saturated

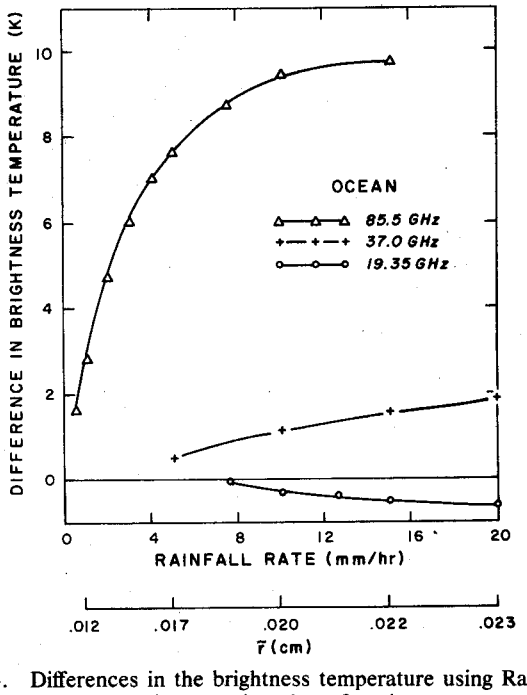

Fig. 3. Differences in the brightness temperature using Rayleigh and Mie scattering phase functions.

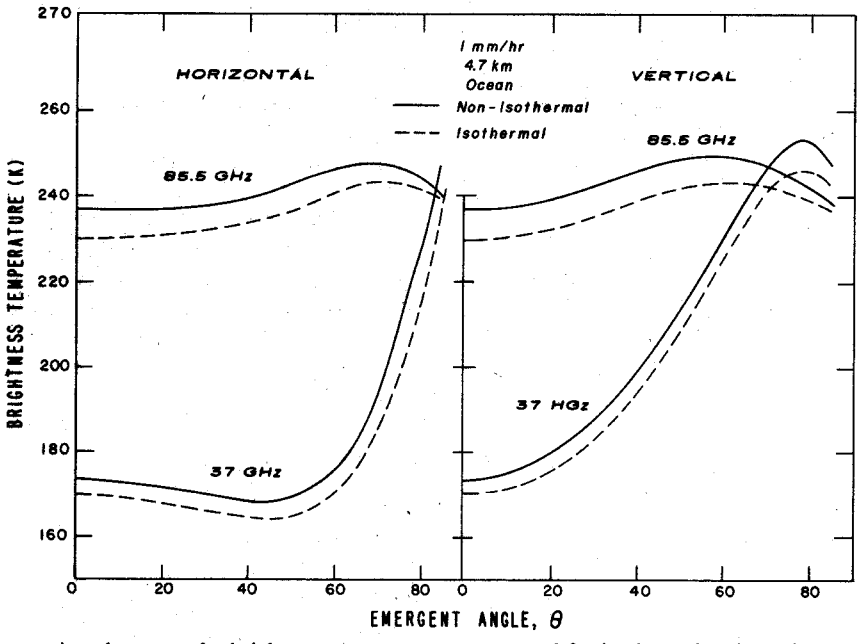

Fig. 4. Comparison between the brightness temperatures computed for isothermal and non-isothermal clouds.

when the rainfall rate reaches a certain value. After saturation the brightness temperature decreases slightly (see Figures 6 and 7) because of the scattering effects of the increasingly large raindrops contained in the heavy precipitating cloud. The increasing rate of the brightness temperature and the critical rainfall rate at which the saturation occurs depend upon the frequency. Based on the present calculations, the saturation rainfall rates for 19.35, 37, and 85.5 GHz are 20, 8, and 2 mm/hr, respectively, for a rain cloud thickness of 4.7 km. Clearly, the brightness temperatures for 19.35 GHz respond to a larger range of the rainfall rate, whereas for 85.5 GHz, variations of the brightness temperature are limited within 2 mm/hr. The relation between the brightness temperature and rainfall rate has been proposed by *Wilheit and Chang* [1977] for determining the rainfall rate over ocean by using the Nimbus 5 ESMR data.

An examination of Figures 5, 6, and 7 also reveals that over ocean the vertical polarized component of the brightness temperature is larger than the horizontal component when the rainfall rates are less than the saturation value. The difference between these two components decreases with increasing rainfall rate. At the saturation point, the two components are nearly equal. Beyond the critical value, the

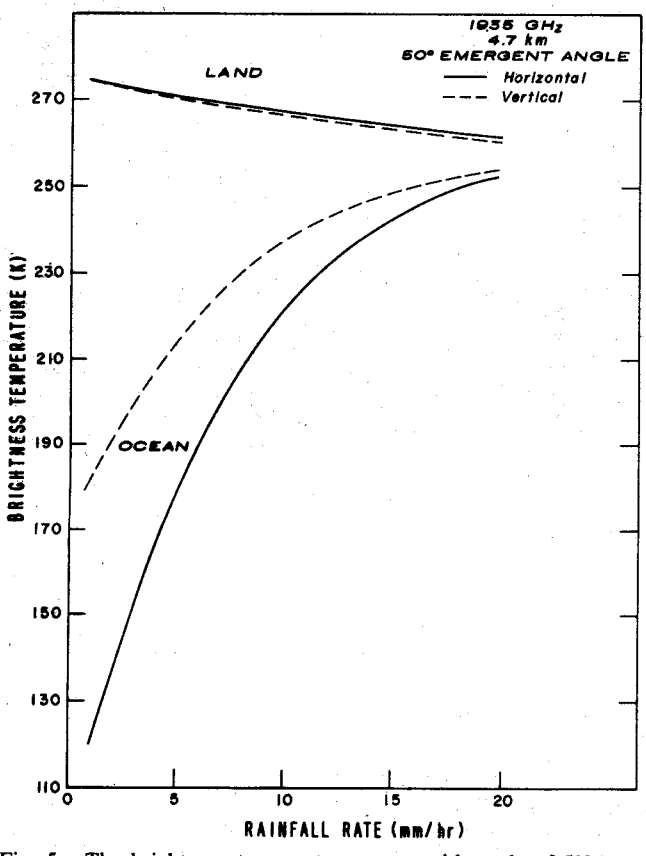

Fig. 5. The brightness temperature at a zenith angle of 50° as a function of the rainfall rate for 19.35 GHz.

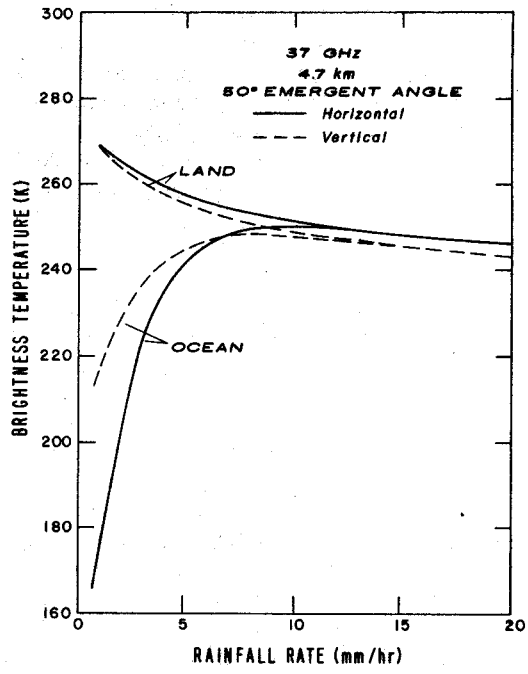

Fig. 6. Same as Figure 5, except for 37.0 GHz.

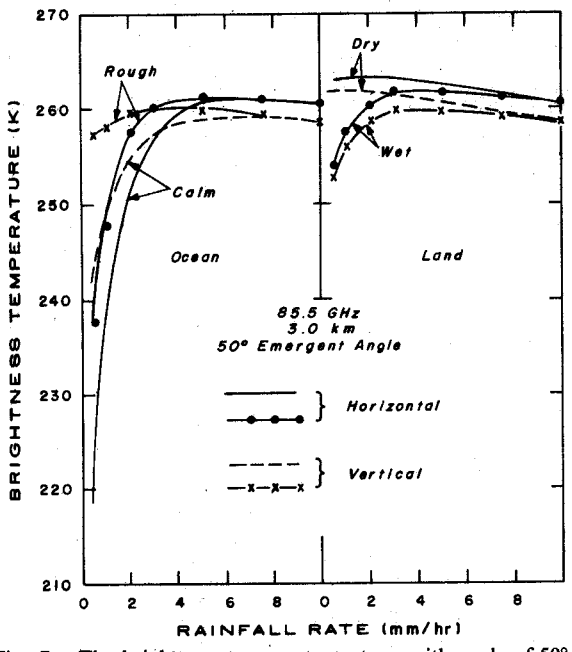

Fig. 7. The brightness temperature at a zenith angle of 50° as a function of the rainfall rate for 85.5 GHz. Effects of the roughening of oceans and the wetting of lands are also shown.

polarization pattern reverses, i.e., the horizontal component becomes larger than the vertical component, and the differences between them are almost constant. This reverse phenomenon is a result of increasing scattering effect of raindrops. It will be presented below that over unpolarized land surfaces, the horizontally polarized brightness temperature is consistently larger than the vertical component.

On the other hand, over the land surface the brightness temperature decreases with increasing rainfall rate. It is seen that the horizontal component is always greater than the vertical component. The difference between them becomes significant for the short wavelength channel (85.5 GHz). The brightness temperature for 85.5 GHz over land is smaller than that for 19.35 GHz for a given precipitation condition. This is due to the fact that strong backscattering of the raindrops takes place at the shorter wavelength. At the zenith angle of 50°, the brightness temperature for 85.5 GHz is about 283.4 K under the clear-air condition, and less than 260 K when precipitation takes place. On the other hand, the brightness temperatures for 19.35 GHz are about 283 K and less than 275 K under clear and precipitation conditions, respectively. Indeed, the response of the rainfall rate to 85.5 and 19.35 GHz is significantly different. The drastic decrease in the brightness temperature at 85.5 GHz under the precipitation conditions may be utilized to explore the feasibility of the rainfall rate determination over the land background. Finally, we note that as the rainfall rate increases the effect of the underlying surface becomes insignificant. This is because the earth surface is covered by a thick cloud of heavy precipitation which is opaque to microwave radiation.

It should be noted that all the foregoing discussions, except Figure 7, utilize the emissivity of calm ocean or dry land. Shown in Figure 7 is a comparison of the brightness temperature of 85.5 GHz between calm and rough oceans and dry and wet lands. As expected, the roughening of the ocean surface increases its emissivity and subsequently increases the brightness temperatures of both polarized components. On the other hand, wetting of the land surface reduces its emissivity and subsequently lowers the brightness temperatures, in light rain conditions. However, as the rainfall rate increases, the influence of the surface emissivity variation on the brightness temperature appears to be less significant because of the large opacity of the heavy precipitation.

In Figures 8, 9, and 10 are shown the linear polarization pattern of the emergent radiation for 19.35, 37, and 85.5 GHz, respectively, for a number of rainfall rates. The degree of polarization shown in these figures is defined as $|TB_l - TB_r|/(TB_l + TB_r)$. The microwave polarization pattern under the clear-air condition is also plotted for comparison purposes. Actually, the degree of polarization for a clear atmosphere represents the polarization characteristics of the ocean surface, because the emission of atmospheric gaseous molecules is unpolarized. It can be seen from these figures that at the nadir direction no polarization is produced in either clear or precipitating conditions. A noticeable feature is that the precipitating cloud over the ocean surface has a depolarization effect. The extent of depolarization depends not only on the rainfall rate, but also on the frequency. For example, at a rainfall rate of 1 mm/hr, a weak depolarization effect is observed for the 19.35 GHz channel. The degree of polarization is seen to be about the same as in the clear-air condition at most angles. A maximum degree of polarization of 30% occurs at the zenith angle of about 65°. For a rainfall rate of 5 mm/hr the maximum polarization is 10%, but the angle at which the maximum polarization occurs shifts to about 60°.

However, for the 37 GHz channel, a rainfall rate of 1 mm/hr appears to have a significant depolarization effect. Figure 9 indicates that the maximum degree of polarization is about 14% which is only half of the maximum polarization under the clear-air condition. For a rainfall rate of 5 mm/hr, which is close to the critical rainfall rate shown in Figure 6,

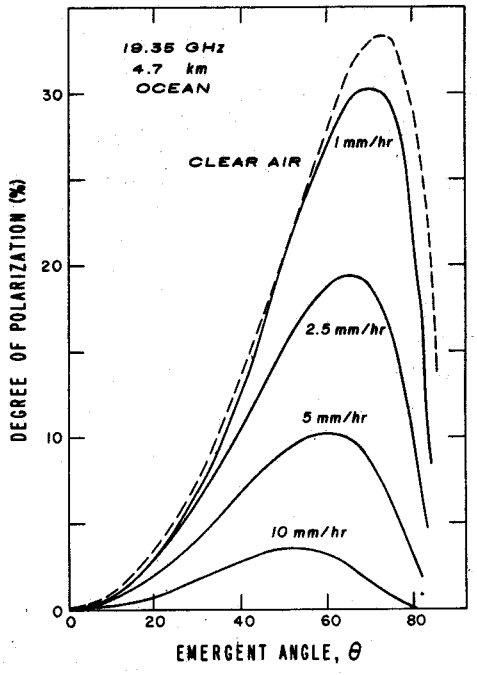

Fig. 8. The degree of linear polarization as a function of the rainfall rate at the top of the atmosphere over an ocean surface for 19.35 GHz.

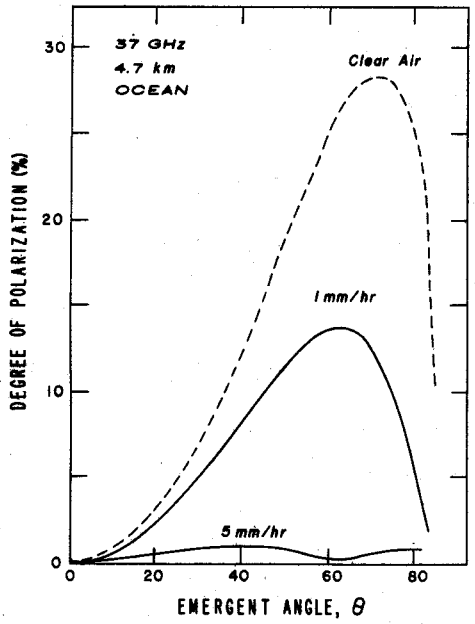

Fig. 9. Same as Figure 8, except for 37.0 GHz.

the maximum polarization is only about 1%. As for 85.5 GHz, the degree of polarization under the clear-air condition is relatively small, and the precipitating cloud has a strong depolarization effect. Even for a small rainfall rate of 1 mm/hr with a thickness of 3 km, the maximum degree of polarization reduces to about 2% for both polarized calm and rough oceans as shown in Figure 10. The slight differences between these two surfaces result from different polarized surface emissivities depicted in Figure 2.

Over the land surface no polarization is produced under the clear air condition because of the unpolarized property of the land surface. Although the Mie scattering of raindrops can produce a slight difference in the two polarization components of the brightness temperature, as shown in Figures 5, 6, and 7, the degree of polarization is rather weak. This allows the possible discrimination between the precipitating condition and the wet land surface which produces significant polarization.

For shorter wavelengths, the possibility of ice particles exists in the upper part of a well-developed precipitating cloud and should be considered in the microwave transfer calculations. Figure 11 illustrates the effect of such an ice layer with various thicknesses on the brightness temperature of 85.5 GHz. The rain layer thickness without ice particles is chosen to be 3 km. While this figure only presents results for the horizontal polarization component, results for the vertical polarization component have the same behavior. The brightness temperature drastically decreases with the rainfall rate when there is an ice layer. This is because in our model the number density of ice particles increases with the rainfall rate which generates a strong scattering effect on the radiation emergent from the precipitating cloud below. This effect has been shown in the theoretical calculations and field observations presented by *Wilheit et al.* [1982].

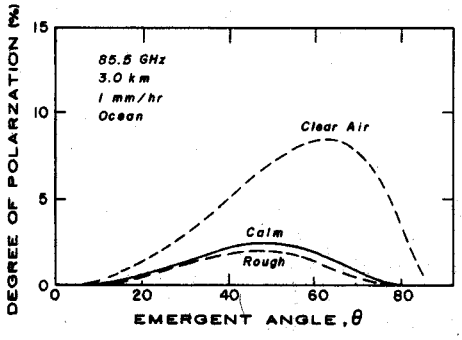

Fig. 10. Same as Figure 8, except for 85.5 GHz.

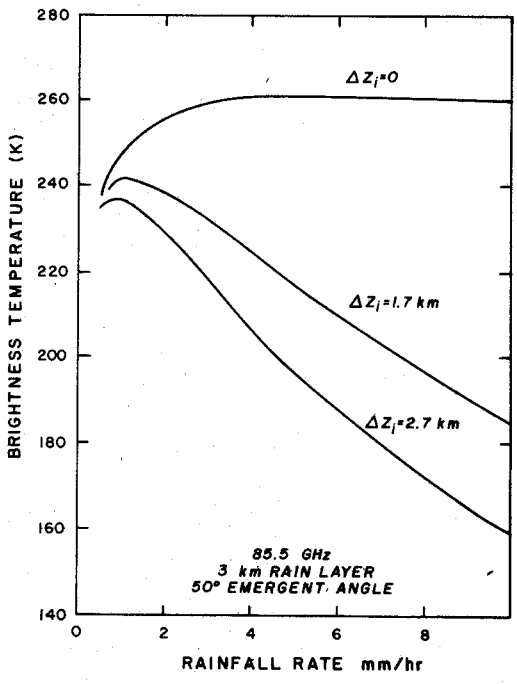

Fig. 11. Effects of an ice layer on the horizontal brightness temperature as a function of the rainfall rate over a rough sea for 85.5 GHz; Δz_i in the figure denotes the thickness of the ice layer.

5. Conclusion

In this paper we have developed a microwave radiation transfer program which takes into account the Mie scattering polarization effect for nonisothermal precipitating clouds in an inhomogeneous atmosphere. This program has been applied to the polarized radiation calculation for three microwave window frequencies of 19.35, 37, and 85.5 GHz, employing a number of rainfall rates and cloud thicknesses over both land and ocean surfaces. Comparisons between brightness temperatures corresponding to Rayleigh and Mie scattering phase functions reveal that the former is a good approximation to microwave radiative processes involving low frequencies (e.g., 19.35 GHz). However, as the rainfall rate and microwave frequency increase the Mie scattering source function must be taken into account in radiative transfer calculations. For example, the calculated brightness temperature for 85.5 GHz, using a Mie scattering phase function, is 7°K larger than that using a Rayleigh scattering approximation for a cloud layer with a thickness of 4.7 km and a rainfall rate of 5 mm/hr. Moreover, we also find that the response range of variations in the brightness temperature to the rainfall rate depends on the frequency. For the frequency of 85.5 GHz, the brightness temperature approaches a saturated value under a precipitating condition of about 2 mm/hr, whereas the saturated rainfall rate for 19.35 GHz is about 20 mm/hr.

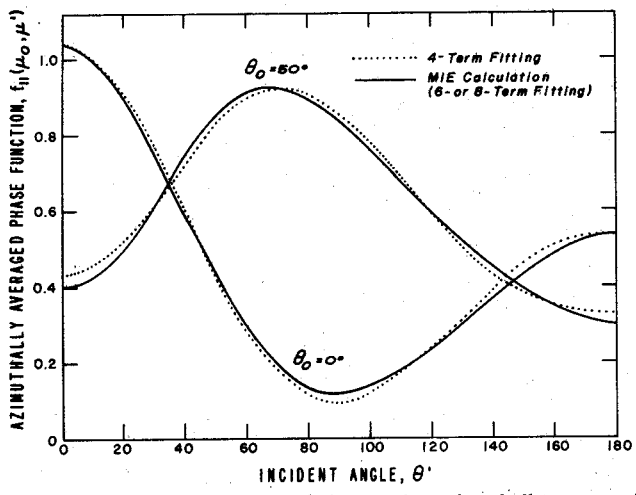

Fig. A1. Double Legendre fitting to the azimuthally averaged Mie scattering phase function for a precipitating cloud with a rainfall rate of 10 mm/hr for 50.31 GHz.

Computational results indicate that the precipitating cloud over a polarized surface (for example, the calm ocean surface) depolarizes the microwave radiation field which strongly depends on the microwave frequency. There is a significant degree of polarization for emergent radiation of 19.35 GHz at a zenith angle of 50° under a light rainfall condition. However, for the frequency of 85.5 GHz, the degree of polarization is less than 1% under the same rainfall condition. Over the unpolarized land surface differences between two polarized components of the brightness temperature produced by precipitating clouds are rather small for the three frequencies used in the calculations. In comparison with the clear-air condition, precipitation produces a drastic decrease in the brightness temperature of 85.5 GHz because of the strong backscattering of raindrops at the shorter wavelength. The essentially unpolarized property coupled with the lower values of the brightness temperature for shorter wavelengths make it more desirable to use 85.5 GHz rather than 37 GHz for discrimination between the light rainfall condition and wet soil surface.

APPENDIX: EXAMINATION OF DOUBLE LEGENDRE POLYNOMIAL EXPANSION AND STABILITY OF EIGENVALUES

We examine the degree of accuracy of the double Legendre expansion described in section 2 to the Mie scattering phase function for microwave wavelengths. Figure A1 shows a comparison of the azimuthally averaged phase function derived from Mie calculations with that of Legendre expansion for a wavelength of 0.594 cm using a 10 mm/hr rainfall rate. For incident zenith angles of 0° and 50° it is seen that six-term expansion fits the Mie phase function with an accuracy within 0.1%.

In the case of Rayleigh scattering, the scattering phase matrix has the following analytical expressions [*Chandrasekhar*, 1960]:

$$M(\theta) = \begin{bmatrix} M_1 & 0 & 0 & 0 \\ 0 & M_2 & 0 & 0 \\ 0 & 0 & M_3 & 0 \\ 0 & 0 & 0 & M_3 \end{bmatrix}$$

$$= \frac{3}{2} \begin{bmatrix} \cos^2\theta & 0 & 0 & 0 \\ 0 & 1 & 0 & 0 \\ 0 & 0 & \cos\theta & 0 \\ 0 & 0 & 0 & \cos\theta \end{bmatrix} \quad \text{(A1)}$$

and the phase matrix elements depicted in (4) are

$$P_{11}(\mu, \mu') = \frac{3}{4}[2(1-\mu^2)(1-\mu'^2) + \mu^2\mu'^2]$$

$$P_{12}(\mu, \mu') = \frac{3}{4}\mu^2 \qquad P_{21}(\mu, \mu') = \frac{3}{4}\mu'^2 \quad \text{(A2)}$$

$$P_{22}(\mu, \mu') = \frac{3}{4}$$

By using the double Legendre polynomials expansion, (A2) can be expressed as

$$P_{11}(\mu, \mu') = \frac{3}{4}P_0(\mu)P_0(\mu') - \frac{1}{2}P_0(\mu)P_2(\mu') - \frac{1}{2}P_2(\mu)P_0(\mu') + P_2(\mu)P_2(\mu')$$

$$P_{12}(\mu, \mu') = \frac{1}{4}P_0(\mu)P_0(\mu') + \frac{1}{2}P_2(\mu)P_0(\mu') \quad \text{(A3)}$$

$$P_{21}(\mu, \mu') = \frac{1}{4}P_0(\mu)P_0(\mu') + \frac{1}{2}P_0(\mu)P_2(\mu')$$

$$P_{22}(\mu, \mu') = \frac{3}{4}P_0(\mu)P_0(\mu')$$

where $P_0(x) = 1$ and $P_2(x) = (3x^2 - 1)/2$ represent Legendre polynomials of zero and second order, respectively.

We have used the numerical procedure developed in this study for the Mie phase function to generate the expansion coefficients for the Rayleigh phase function and have found that they are identical to those given in (A3). On substituting (A3) into the discrete ordinates differential equations, numerical solutions for the Rayleigh scattering phase function may be obtained. Comparison with the analytic solution given by *Liou et al.* [1980] shows that the agreement of the resulting calculations are better than 1%.

In order to derive the general solution of the homogeneous equations for the system of discrete-ordinates equations, we first apply the standard matrix method developed by *Liou* [1973] to get the eigenvalues in the form

$$f(k) = k^{4N} + d_1k^{4N-1} + \cdots + d_{4N-1}k + d_{4N} = 0 \quad \text{(A4)}$$

where coefficients d_j are related to the trace of the coefficient matrix of the homogeneous equations. In Liou's paper, the stability of eigenvalues was discussed. Recently, *Stamnes and Swanson* [1981] have improved the standard matrix method by searching the roots of the polynomial of k^2 instead of k on the basis of the symmetry of the phase function. The azimuthally averaged phase function matrix elements for spherical particles developed in this paper have the symmetrical relationships as follows:

$$P_{rs}(\mu_i, \mu_j) = P_{rs}(\mu_j, \mu_i) \qquad i, j = 1, 2, \cdots, 2N$$
$$P_{rs}(\mu_{N+1-n}, \mu_{N+1-n}) = P_{rs}(\mu_{N+n}, \mu_{N+n}) \qquad n = 1, 2, \cdots, N \tag{A5}$$

Because of these symmetrical characteristics, the first coefficients d_1 in (A4) will become zero. Other odd coefficients can also be proven to be zero elements numerically. Consequently, (A4) will contain polynomials in k^2 which will give real positive and negative roots.

Acknowledgments. This research was supported in part by the Division of the Atmospheric Sciences, National Science Foundation under grant ATM-81-09050. We thank Sharon Bennett for typing and editing the manuscript.

REFERENCES

Barrett, A. H., and V. K. Chung, A method for the determination of the high-altitude water vapor abundance from ground-based microwave observations, *J. Geophys. Res., 67*, 4259–4266, 1962.

Chandrasekhar, S., *Radiative Transfer*, Dover, New York, 1960.

Dave, J. V., Intensity and polarization of the radiation emerging from a plane-parallel atmosphere containing monodispersed aerosols, *Appl. Opt., 9*, 2673–2684, 1970.

Gaut, N. E., Studies of atmospheric water vapor by means of passive microwave techniques, *Tech. Rep. 467*, Mass. Inst. of Technol. Res. Lab. Electron., Cambridge, 1968.

Gloersen, P., T. Wilheit, and T. Schmugge, Microwave emission measurements of sea surface roughness, soil moisture and sea ice structure, *4th Annual Earth Resources Program Review*, vol. 1, NASA, 1972.

Hall, F. G., Microwave brightness temperature of a windblown sea, *4th Annual Earth Resources Program Review*, vol. 1, NASA, 1972.

Liou, K. N., A numerical experiment on Chandrasekhar's discrete-ordinate method for radiative transfer: Applications to cloudy and hazy atmospheres, *J. Atmos. Sci., 30*, 1303–1326, 1973.

Liou, K. N., *An Introduction to Atmospheric Radiation*, Academic, New York, 1980.

Liou, K. N., H. Y. Yeh, F. M. Chen, K. Hutchison, and E. Astling, Development of infrared and microwave techniques for cloud parameter inference from satellite imagery and sounder data, *Final Rep. AFGL-TR-80-0263*, Air Force Geophys. Lab., Bedford, Mass., 1980.

Marshall, J. S., and W. M. Palmer, The distribution of raindrops with size, *J. Meteorol., 5*, 165–166, 1949.

Meeks, M. L., and A. E. Lilley, The microwave spectrum of oxygen in the earth's atmosphere, *J. Geophys. Res., 68*, 1683–1703, 1963.

Ray, P. S., Broadband complex refractive indices of ice and water, *Appl. Opt., 11*, 1836–1844, 1972.

Stamnes, K., and R. A. Swanson, A new look at the discrete-ordinate method for radiative transfer calculations in anisotropically scattering atmospheres, *J. Atmos. Sci., 38*, 387–399, 1981.

Webster, W. J., T. T. Wilheit, D. B. Ross, and P. Gloersen, Spectral characteristics of the microwave emission from a wind-driven foam-covered sea, *J. Geophys. Res., 81*, 3095–3099, 1976.

Weinman, J. A., and P. J. Guetter, Determination of rainfall distribution from microwave radiation measured by the Nimbus 6 ESMR, *J. Appl. Meteorol., 16*, 437–442, 1977.

Wilheit, T. T., and A. T. C. Chang, A satellite technique for quantitatively mapping rainfall rates over the oceans, *J. Appl. Meteorol., 16*, 551–559, 1977.

Wilheit, T. T., et al., Microwave radiometric observations near 19.35, 92, and 183 GHz of precipitation in tropical storm Cora, *J. Appl. Meteorol., 21*, 1137–1145, 1982.

(Received June 17, 1982;
revised January 7, 1983;
accepted January 7, 1983.)